Substitution of Y, Ce, and Th for La in $LaBeH_8$ as a path towards lower synthesis pressures of superconducting hydrides

Yuan Ma,[1] Jie Luo,[1] Sheng Meng,[2] Xin Zhong,[1,*] Guangtao Liu,[1,†] Hanyu Liu,[1,3,‡] and Yanming Ma[1,3]

[1]*Key Laboratory of Material Simulation Methods and Software of Ministry of Education and State Key Laboratory of Superhard Materials, College of Physics, Jilin University, Changchun 130012, China*

[2]*Institute of Physics, Chinese Academy of Sciences, Beijing 100190, China*

[3]*International Center of Future Science, Jilin University, Changchun 130012, China*

(Received 19 July 2024; revised 11 April 2025; accepted 16 April 2025; published 15 May 2025)

Recent theory-guided discoveries of hydrides exhibiting high superconducting temperatures (T_c) exceeding 200 K above 150 GPa have sparked the enthusiasm for the pursuit of room-temperature ambient-pressure superconductors. While efforts to increase the T_c's of these hydrides are underway, optimizing the demanding high-pressure synthesis conditions remains a challenge. Several studies suggested that a multielemental alloying strategy could be a feasible approach to tackle this formidable task. Here, we present an example using $LaBeH_8$ to establish several alloy hydrides via the substitution of La atoms with similar metal atoms, such as Y, Ce, and Th. Quasiquaternary alloy hydride (La, Y, Ce, Th)BeH_8 is computed to become thermodynamically stable at 70 GPa and a typically realistic temperature of ~2000 K for synthesizing high-T_c hydrides, compared with the calculated results showing thermodynamic instability above 300 GPa without considering entropy. Our in-depth analysis revealed that not only does entropy play a crucial role in stabilizing alloy hydrides at moderate pressures and high temperatures, but also the energy contribution from vibrational entropy is much more significant than configurational entropy, where configurational entropy has long been believed to play a key role in the stability of multielemental alloy. Furthermore, extensive electron-phonon simulations indicate that the estimated T_c of (La, Y, Ce, Th)BeH_8 could reach near ~100 K at 70 GPa. The present work offers a fresh perspective on the design and realization of high-T_c multielemental alloy hydrides towards near-ambient pressure.

DOI: 10.1103/PhysRevB.111.184512

I. INTRODUCTION

Over the past decade, the search for high-temperature superconductivity in the hydrogen-rich system has garnered great interest due to the findings of a critical temperature (T_c) above 200 K in numerous hydrides [1–6], such as covalent H_3S [7,8] and clathrate hydrides (CaH_6 [9,10], YH_6, YH_9 [11,12], LaH_{10} [13,14], etc.) under pressures above 150 GPa. However, lowering the synthesis pressure of these fascinating hydrides, which is critical to pursuing high-temperature superconductivity at relatively low or even ambient pressure, presents a formidable task. Towards this goal, considerable efforts have been devoted to the exploration of superconducting hydrides at submegabar pressures [15–19]. For example, several studies have predicted that high-T_c LaXH$_8$ (X = B, Be) [20–22] could be thermodynamically stable above 100 GPa, especially as their dynamically stable pressure could reach as low as 50 GPa. Motivated by these predictions, a recent experiment indeed successfully synthesized $LaBeH_8$ with a T_c of 110 K at megabar pressure, and this phase could be maintained upon decompression to at least 80 GPa [23]. Recently, a type of ambient-pressure hydride superconductor Mg_2IrH_6 with the highest T_c up to 160 K was proposed, while the metastable feature of this structure results in great challenges for further experimental synthesis [24,25]. These studies indicate that not only is thermodynamically stable pressure key for low-pressure synthesis of a hydride, but also the search for high-temperature superconducting hydrides at moderate pressures remains a pressing task.

It is widely recognized that most experimental syntheses often involve high-temperature conditions, where the contribution of entropy to Gibbs free energy is apparently more pronounced. Particularly in disordered multinary systems, configurational entropy even overwhelms the mixing formation enthalpy, thereby driving their formation [26,27]. Consequently, multielemental alloy hydrides may become thermodynamically stable at moderate pressures and high temperatures due to the reduction of Gibbs free energy facilitated by the increasing configurational entropy of the multinary system. This idea is exemplified by synthesizing quasibinary (La, Y)H_4 alloy hydride at ~110 GPa and 2200 K, which is much superior to YH_4 synthesized above 143 GPa [28]. In addition, there are some other studies hunting for quasibinary [29–35], even quasiternary [36] alloy hydrides, in which computationally unstable structures ($Im\bar{3}m$-LaH_6 [30], $P6_3/mmc$-LaH_9 [31,32], and $Fm\bar{3}m$-YH_{10} [30,36]) all could be observed by the introduction of additional metal elements. Therefore, the search for thermodynamically stable multielemental high-T_c alloy hydrides at lower

*Contact author: zhongxin@calypso.cn
†Contact author: liuguangtao@jlu.edu.cn
‡Contact author: hanyuliu@jlu.edu.cn

pressures is feasible and highly required in this hot domain of science.

The experimental study has shown that $LaBeH_8$ exhibits the highest T_c of 110 K at ~80 GPa [23], which is above the liquid nitrogen temperature of 77 K. Moreover, many theoretical studies tried to lower dynamically stable pressures for the compounds isostructural to $LaBeH_8$ [37–42]. It is natural to wonder if the thermodynamically stable pressure of this $LaBeH_8$-like prototype structure could be further lowered via doping additional metal elements that introduce considerable entropy at typically realistic temperature, such as ~2000 K, for synthesizing high-temperature superconducting hydrides. To this end, we conducted thorough simulations by mixing Y, Ce, and Th at La sites in $LaBeH_8$. As a result, (La, Ce)BeH_8, (La, Th)BeH_8, and (La, Ce, Th)BeH_8 are calculated to be thermodynamically stable at significantly lower pressures of 77, 66, and 60 GPa, respectively, by additionally considering entropy at 2000 K. Especially for multielemental alloy (La, Y, Ce, Th)BeH_8, entropy assists maintaining thermodynamically stable down to 70 GPa from several megabars. Furthermore, we also conducted a comprehensive study on the impact of vibrational entropy and configurational entropy on thermodynamic stability. Finally, detailed electron-phonon coupling simulations are performed for these multielemental alloy structures, and the estimated T_c's of (La, Ce)BeH_8, (La, Th)BeH_8, (La, Ce, Th)BeH_8, and (La, Y, Ce, Th)BeH_8 could reach 53, 83, 49, and 87 K at their lowest thermodynamically stable pressures of 77, 66, 60, and 70 GPa, respectively. Our current research on alloy hydrides shows that the thermodynamic stability of multielemental alloy hydrides depends on the competition between mixing formation enthalpy and entropy, which serves as a valuable reference for future experimental endeavors towards the ultimate goal of achieving high-temperature superconductivity at ambient pressure.

II. COMPUTATIONAL DETAILS

The energetic calculations in our study were carried out by employing the Vienna *Ab initio* Simulation Package (VASP) [43], which is based on density-functional theory [44] within the generalized gradient approximation in the form of the Perdew-Burke-Ernzerhof [45] exchange-correlation functional. The electron-ion interaction is described by all-electron projector-augmented wave (PAW) [46] method, wherein $5s^2\,5p^6\,5d^1\,6s^2$, $4s^2\,4p^6\,4d^1\,5s^2$, $4f^1\,5s^2\,5p^6\,5d^1\,6s^2$, $5f^1\,6s^2\,6p^6\,6d^1\,7s^2$, $1s^2\,2s^2$, and $1s^1$ serve as the valence electrons for La, Y, Ce, Th, Be, and H, respectively. The kinetic cutoff energy for plane-wave basis set with 900 eV and Monkhorst-Pack k meshes with a resolution of 0.18 $Å^{-1}$ are utilized to ensure the enthalpy converges well. The formation enthalpy of all alloy structures against the decomposition paths are calculated by PYMATGEN [47].

Bonding in these hydrides was analyzed by the crystal orbital Hamiltonian population (COHP) [48,49] implemented in LOBSTER code [50]. The Bader charge analysis [51] was used to investigate charge transfer, and the electron localization function (ELF) [52] was used to visualize chemical bonds in molecules and solids. The lattice dynamics and electron-phonon coupling of the stable structures are calculated within the framework of density-functional perturbation theory [53] through the QUANTUM-ESPRESSO code [54], where PAW pseudopotentials were adopted with a kinetic energy cutoff of 80 Ry. Self-consistent electron density and electron-phonon coupling (EPC) were calculated by employing 16 × 16 × 16 k-point meshes and 4 × 4 × 4 q-point meshes for *Pmmm* phase; 20 × 20 × 16 and 5 × 5 × 4 for *P4/mmm* phase; and 12 × 16 × 16 and 3 × 4 × 4 for *P*1 phase. The superconducting gap and T_c value were calculated by numerically solving the isotropic Eliashberg equations [55–57] with the ELK code [58].

To examine the energy stability of the substitutional alloy (La, Y, Ce, Th)BeH_8, it was modeled by using a supercell of 160 atoms based on the special quasirandom structures (SQS) approximation [59] as implemented in the ALLOY THEORETIC AUTOMATED TOOLKIT [60]. Based on the unit cell of $Fm\bar{3}m$ $LaBeH_8$ containing 40 atoms, the La sites was randomly occupied by La, Y, Ce, and Th in equiatomic ratio to create an SQS supercell with 160 atoms.

The configurational entropy under ideal mixing conditions is calculated by

$$S_{\text{conf}} = -k_B \sum_{i=1}^{N} x_i \ln x_i, \tag{1}$$

where k_B is the Boltzmann constant, N is the number of component, and x_i represents the atomic fraction of component i on the site of mixing. Furthermore, the Boltzmann constant is related to the gas constant R through $R = k_B N_A$, where N_A is Avogadro's constant. As an example, in the fcc structure ($Fm\bar{3}m$) of $LaBeH_8$ where La atoms occupy 4b site, the configurational entropy of four-element equimolar alloy mixing at 4b site is $1.386k_B$ per La site, and $0.139k_B$ per atom. Therefore, the contribution of configurational entropy of (La, Y, Ce, Th)BeH_8 to Gibbs free energy at a typical temperature of 2000 K is 23.8 meV per atom. The vibrational contribution to the free energy can be estimated by *ab initio* methods, requiring the calculation of the interatomic force constants in a large supercell. Phonon calculations were carried out using a supercell approach as implemented in PHONOPY code [61]. The vibrational energy and entropy were obtained from lattice dynamic calculations using the quasiharmonic approximation. In this approximation, the vibrational free energy takes the form [62]

$$F_{\text{vib}} = \sum_{i}^{3N} \left[\frac{\hbar\omega_i}{2} + k_B T \ln(1 - e^{-\hbar\omega_i/k_B T}) \right], \tag{2}$$

where ω is the phonon vibrational frequency. And, the vibrational entropy by differentiating with respect to T is

$$S_{\text{vib}} = k_B \sum_{i}^{3N} \left[-\ln(1 - e^{-\hbar\omega_i/k_B T}) + \frac{\hbar\omega_i/k_B T}{e^{-\hbar\omega_i/k_B T} - 1} \right]. \tag{3}$$

Furthermore, we also have made the approximation that the electronic entropy contribution to the Gibbs free energy is neglected compared to the phonon contribution.

Ab initio molecular dynamics (AIMD) simulations for (La, Y, Ce, Th)BeH_8 were performed with the same pseudopotentials and exchange-correlation functional as those used in the geometrical optimization. The cutoff energy was

reduced to 537.5 eV with an energy convergence criterion of 1×10^{-4} eV, and the Brillouin-zone k point was chosen as the Γ point. The simulated systems contained 320 atoms generated by SQS approximation, which were heated in Nosé-Hoover thermostats (300, 2000, 2500, and 3000 K) based on the *NVT* ensemble [63–65] at 70 GPa. The simulation duration was 11 ps (22 000 steps × 0.5 fs per step), with the statistical information of mean-square displacements and atomic trajectories extracted from the last 10 ps.

The training data for the deep-learning potential model were obtained from *ab initio* molecular dynamics simulations at 300 K. An equiatomic 5 × 5 × 5 supercell containing 5000 atoms was constructed from a unit cell with 40 atoms relaxed at 70 GPa, and then atomic sites of La, Y, Ce, and Th were randomly shuffled. At each time step, all atom pairs of heavy elements (La, Y, Ce, and Th) are swapped once. A Nosé-Hoover thermostat was adopted to perform the *NVT* ensemble with a temperature of 300 K for the first 10 ps, followed by lengthy MC/MD (Monte Carlo/molecular dynamics) replica exchange simulations [66] for 90 ps by using the LAMMPS software package [67,68].

A simple expression for the configurational entropy of mixing, developed by Hanke *et al.* [69], which relies solely on the set of instantaneous coordinates, was employed to assess the degree of mixing along a molecular dynamics trajectory. We extended their formula to alloys with four disorderedly occupied elements:

$$\Delta S_{\text{conf}} = \sum_{\alpha=1}^{N} \Delta S_{\alpha}, \tag{4}$$

$$\Delta S_{\alpha} = -k_B\left(x_{\alpha}^{(A)} \ln x_{\alpha} + x_{\alpha}^{(B)} \ln x_{\alpha} + x_{\alpha}^{(C)} \ln x_{\alpha} + x_{\alpha}^{(D)} \ln x_{\alpha}\right) \tag{5}$$

where ΔS_{α} is mixing entropy in elementary volumes V_{α} that is obtained by dividing total volume into N small elementary volumes. As entropy is an extensive quantity, the total entropy of mixing of the entire ΔS_{conf} can be written as the sum over the entropies of mixing, ΔS_{α}. Here, $x_{\alpha}^{(A)}$ is the molar fraction of species A in the elementary volume element V_{α}.

Hanke *et al.* proposed molar fraction distributions based solely on the partial densities of the four species $\rho^{(A)}(r)$, $\rho^{(B)}(r)$, $\rho^{(C)}(r)$, and $\rho^{(D)}(r)$ via

$$x^{(A)}(r) = \frac{\rho^{(A)}(r)}{\rho^{(A)}(r) + \rho^{(B)}(r) + \rho^{(C)}(r) + \rho^{(D)}(r)}, \tag{6}$$

where r is atomic coordinates in real space. They defined the $\rho^{(A)}(r)$ via a Gaussian function of actual atomic coordinates of the particles R_i:

$$\rho_i(r) = \frac{1}{\left(\sqrt{2\pi}\sigma\right)^3} \exp\left[-\frac{(r-R_i)^2}{2\sigma^2}\right], \tag{7}$$

$$\rho^{(A)}(r) = \sum_{i \epsilon A} \rho_i(r). \tag{8}$$

III. RESULTS AND DISCUSSION

A. Thermodynamical properties

We begin our first-principles simulations on the experimentally synthesized $LaBeH_8$-type structure by substituting La atoms with three different elements with considering configurational entropy at 2000 K. The primary assumption is that mixed heavy elements (La, Y, Ce, and Th) with different ratios can achieve an ideal, uniformly disordered state, while the fcc metal lattice remains almost unchanged without melting [see Fig. 4(a)]. Therefore, we can apply the ideal configurational entropy formula (1) to compute its contribution to the free energy at 2000 K. The results show that the combinations of La/Th, La/Ce, and Ce/Th for quasibinary alloy hydrides can maintain thermodynamic stability within megabar pressure at 2000 K. For example, (La, Th)BeH_8 with an equal mole of La and Th is thermodynamically stable at a much lower pressure of 91 than ∼110 GPa as for $LaBeH_8$ at 2000 K in the top panel of Fig. 1(a). Additionally, (La, Ce)BeH_8 also can maintain thermodynamic stability under pressures of 99 GPa at 2000 K, which motivated us to investigate quasiternary and quasiquaternary alloy hydrides. As a consequence, (La, Ce, Th)BeH_8 are computed to be thermodynamically stable above 87 GPa at 2000 K, and the quasiquaternary alloy hydride (La, Y, Ce, Th)BeH_8 exhibits thermodynamic stability above 123 GPa at 2000 K in the present study [the top panel of Fig. 1(a)]. The complete calculation results for free energies with respect to pressure of other alloys are described in Appendix B (including Refs. [70–72]). Our findings demonstrate that configurational entropy drives the multielemental alloys to maintain thermodynamic stability at typical experimental temperatures (2000 K) within megabar pressure. However, as the pressure decreases, the contribution of the mixing formation enthalpy rises significantly, and it is necessary to investigate if other physical factors could further reduce the thermodynamically stable pressure.

The hydrides mentioned above were considered as a superconducting alloy composed of a distorted BeH_8 sublattice and randomly substituted metal sublattice as shown in typical (La, Y, Ce, Th)BeH_8 (Fig. 2) akin to the high-entropy ceramics. To examine the influence of the cell size and configurational disorder on energy stability as reported in (Y, Sr)H_{22} [73], in this study we took (La, Y, Ce, Th)BeH_8 as a representative example to perform the quasirandom structure (SQS) simulations, the best way to mimic a substitutional alloy structure, to check if the crystal-structure model with the simulated cell of 40 atoms is accurate enough to describe the system, before any further analysis. We thus carried out structural relaxations at a representative pressure of 100 GPa and found that the energy variations among these quasirandom structures (the unit cells of 40 and 160 atoms) were within an energy deviation of ∼2 meV per atom (Fig. 3). This indicates that cell size does not apparently affect the study of the structure of (La, Y, Ce, Th)BeH_8. Therefore, the unit-cell structures listed in Appendix A were employed to study the electronic and phononic properties, as well as superconductivity for (La, Y, Ce, Th)BeH_8, along with other quasibinary and quasiternary alloy hydrides in the following studies.

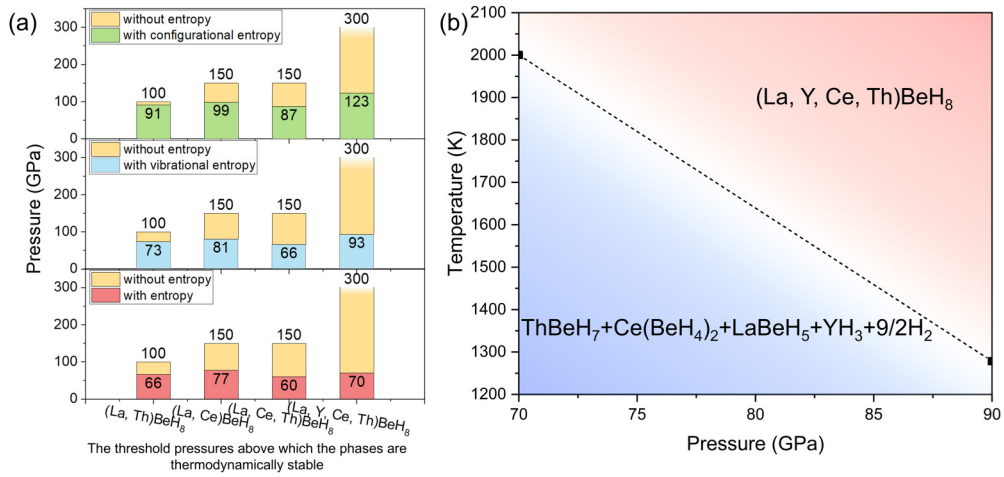

FIG. 1. (a) Comparison of the lowest thermodynamically stable pressures in alloy hydrides with or without different entropy effects. Yellow bars represent the lowest thermodynamically stable pressures at 0 K, while green, blue, and red bars correspond to the lowest thermodynamically stable pressures at 2000 K, when configurational, vibrational entropy or both are included, respectively. It is noted that (La, Y, Ce, Th)BeH_8 is thermodynamically unstable even at 300 GPa. (b) Pressure-temperature phase diagram of (La, Y, Ce, Th)BeH_8 by considering the contribution of configurational and vibrational entropy.

Then, we estimated the melting point of the most relevant quasiquaternary system (La, Y, Ce, Th)BeH_8 to verify the validity of the configurational entropy formula at 2000 K. The simplest simulation approach to investigate the melting behavior of alloy materials is to heat the solid phase until melting. The corresponding calculated melting temperature (T_+) is regarded as melting temperature (T_M), but T_+ is always higher than T_M. The mean-square displacements (MSDs) indicated that the metal fcc lattice in (La, Y, Ce, Th)BeH_8 does not undergo melt or dissociation at 2000 K. Instead, only the hydrogen atoms dissociate and migrate at high temperatures [Fig. 4(a)]. La, Y, Ce, and Th begin to exhibit complete migration at 2500 and 3000 K, indicating the occurrence of melting [Figs. 4(b) and 4(c)]. These results suggest our approximation for disordered occupation of the heavy-metal positions is reasonable, and the ideal configurational entropy of the system could be estimated.

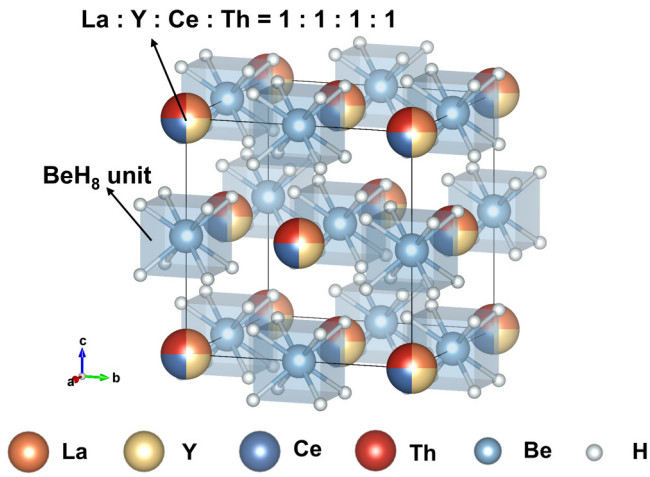

FIG. 2. Alloy structure of (La, Y, Ce, Th)BeH_8. Orange, yellow, dark blue, red, dusty blue, and gray spheres represent La, Y, Ce, Th, Be, and H atoms, respectively.

In order to estimate configurational entropy better, we adopted machine-learning potential to perform the MC/MD simulations at 300 K. Lengthy MC/MD replica exchange simulations were performed until they reached equilibrium at 300 K, as judged by time series of energies [Fig. 4(d)]. As shown in Fig. 4(e), the simulation was initiated with artificially disordered phases, and its configurational entropy was approximately 1.353R. During our MC/MD simulation, the configurational entropy slightly increased to 1.367R, approaching an ideal value of ln 4R (1.386R), which represents an equiatomic mixture of La, Y, Ce, and Th. Figure 4(f) shows that the distorted BeH_8 units remain undamaged, and the entire structure maintains its kinetic stability. The reason we did not perform replica exchange MC/MD simulation at higher temperatures is that hydrogen atoms begin to diffuse, resulting in more complex atomic local environments. It requires an exceptionally longer time to run active training of the machine-learning potential for (La, Y, Ce, Th)BeH_8, which is beyond the scope of the current work.

It is known that configurational entropy has been long believed to play a key role in the stability of multielemental alloy. However, in addition to configurational entropy, vibrational entropy should be considered for a comprehensive study of the stability of the alloy system at high temperatures. We then compared the effect of configurational and vibrational entropy on the thermodynamic stability in the aforementioned alloy hydrides. The results show that the thermodynamically stable pressures considering vibrational entropy are several tens of GPa lower than those considering configurational entropy in the middle panel of Fig. 1(a). Motivated by these unexpected results, we further estimated the thermodynamically stable pressures of these predicted alloy hydrides by considering both vibrational and configurational entropy, as shown in the bottom panel of Fig. 1(a), such as (La, Th)BeH_8 (66 GPa at 2000 K) and (La, Ce)BeH_8 (77 GPa at 2000 K). Regarding (La, Ce, Th)BeH_8 and (La, Y, Ce, Th)BeH_8, they can maintain thermodynamic stability above 60 and 70 GPa, respectively, at 2000 K. More

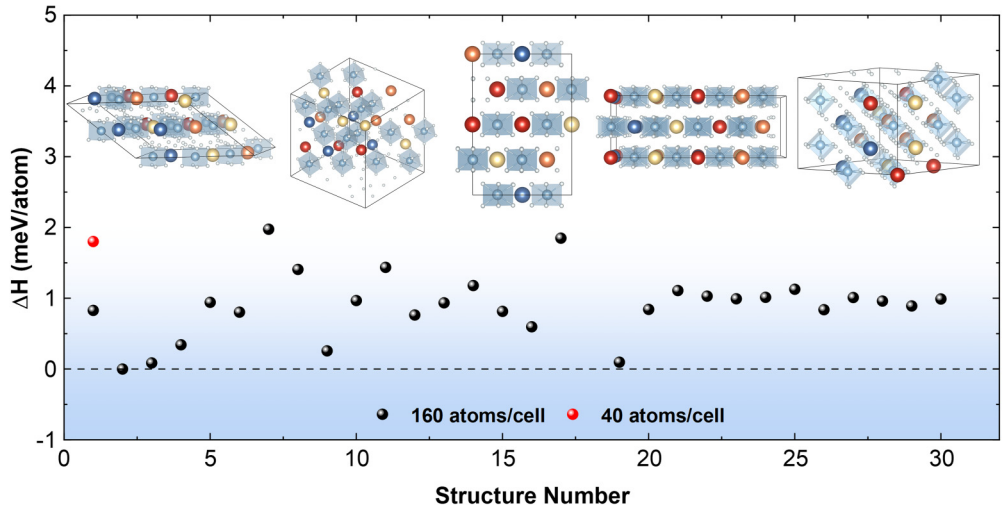

FIG. 3. The calculated enthalpy of (La, Y, Ce, Th)BeH_8 with different assignments of La, Y, Ce, and Th atoms to SQS site classes at 100 GPa, where the SQS supercells with 160 atoms display five distinct typical lattice configurations.

results are shown in Fig. 5. These results indicate that the contribution of vibrational entropy to thermodynamic stability for alloy cannot be overlooked at high temperatures. Moreover, we also provide the pressure-temperature phase diagram of (La, Y, Ce, Th)BeH_8 [Fig. 1(b)], which indicates that the entropy effect can indeed optimize the stable pressures of multicomponent alloys with increasing temperature.

To elucidate the origin of substantial energy contribution from vibrational entropy in these multielemental alloy hydrides, we conducted a thorough comparison of the bonding behaviors and vibrational modes for (La, Y, Ce, Th)BeH_8 and $LaBeH_8$. In $LaBeH_8$, the mid- to high-frequency phonon vibrational modes are associated with both intra-BeH_8 and inter-BeH_8 vibrations, and most vibrational modes are degenerate due to the high symmetry [74]. However, the Be–H bond

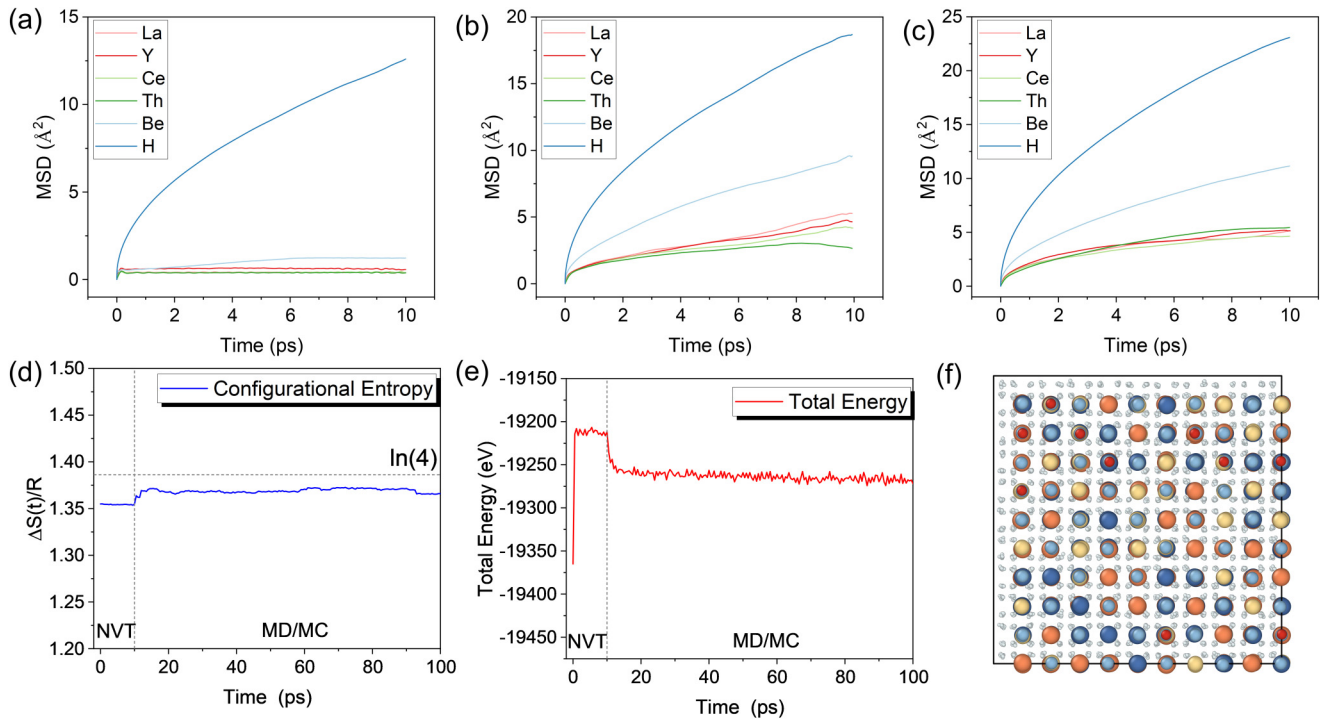

FIG. 4. Mean-square displacements (MSDs) for alloy hydrides (La, Y, Ce, Th)BeH_8 obtained by AIMD calculations in the *NVT* ensemble at (a) 2000 K, (b) 2500 K, and (c) 3000 K, respectively. Evolution of the (d) total energy and (e) instantaneous configurational entropy of (La, Y, Ce, Th)BeH_8 during the MC/MD simulations at 300 K, where R is the gas constant. The simulation is conducted in the *NVT* ensemble for the first 10 ps, followed by MC/MD replica exchange simulations. (f) The disorder configuration of (La, Y, Ce, Th)BeH_8 at 100 ps. Orange, yellow, dark blue, red, dusty blue, and gray spheres represent La, Y, Ce, Th, Be, and H atoms, respectively.

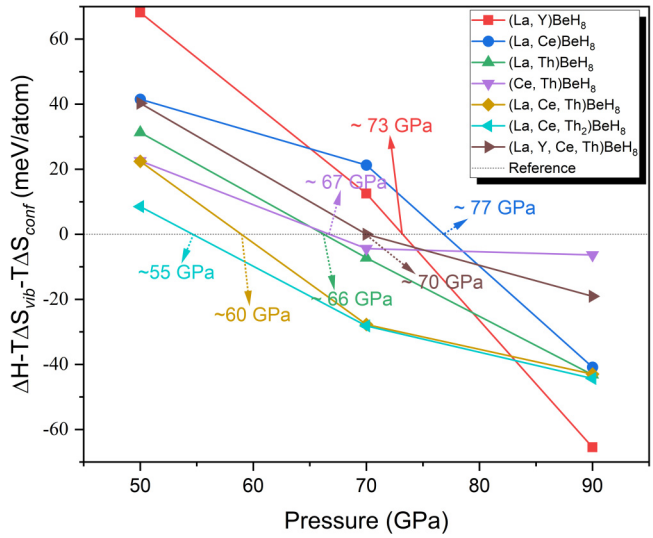

FIG. 5. Calculated Gibbs free energy for (La, Y)BeH_8, (La, Ce)BeH_8, (La, Th)BeH_8, (Ce, Th)BeH_8, (La, Ce, Th)BeH_8 (La, Ce, Th_2)BeH_8, and (La, Y, Ce, Th)BeH_8 as a function of pressure considering the contribution of configurational entropy (ΔS_{conf}) and vibrational entropy (ΔS_{vib}) at pressure-temperature conditions of 50–90 GPa and 2000 K.

length in (La, Y, Ce, Th)BeH_8 exhibits large deviation as a result of the disordered occupations of metal atoms [Fig. 6(a)], which results in the breaking of the degenerate vibrational modes of BeH_8. Compared to $LaBeH_8$, all vibrational modes of (La, Y, Ce, Th)BeH_8 exhibit non-degeneracy (Appendix C), and the expanded broadening of phonon density of states in (La, Y, Ce, Th)BeH_8 implies a higher level of vibrational disorder [Fig. 6(b)]. Our simulations also indicated that the Gibbs free energy considering vibrational entropy of (La, Y, Ce, Th)BeH_8 is −48 meV per atom at 2000 K and 70 GPa with respect to the lowest decomposition into $ThBeH_7$, $Ce(BeH_4)_2$, $LaBeH_5$, YH_3, and $9/2H_2$. Additionally, as the number of atoms increases in the supercell of (La, Y, Ce, Th)BeH_8, the distortion of Be–H bonds and BeH_8 units becomes more pronounced [Fig. 6(a)], as reported in other systems [75]. These results indicate that the distortion of the BeH_8 cubic units is the underlying mechanism for a significant contribution stemming from vibrational entropy.

B. Lattice dynamics

It is known that the thermodynamically stable pressure of these alloy structures at 0 K could be higher than that at 2000 K, where entropy plays a key role in stabilizing the system at high temperatures. However, these alloy structures might be retained through rapid quenching from high-temperature conditions, since they can exhibit dynamic stability at low pressures. Therefore, we performed dynamical simulations on the proposed alloy structures, and the corresponding phonon spectra at their lowest dynamically stable pressures are illustrated in Fig. 7 [and see Fig. 11(a)]. In general, quasibinary alloy hydrides can maintain dynamic stability below 20 GPa or even near 10 GPa, while (La, Ce, Th)BeH_8 and (La, Y, Ce, Th)BeH_8 require high pressures of 30 and 32 GPa, respectively. For the simulations of critical dynamical

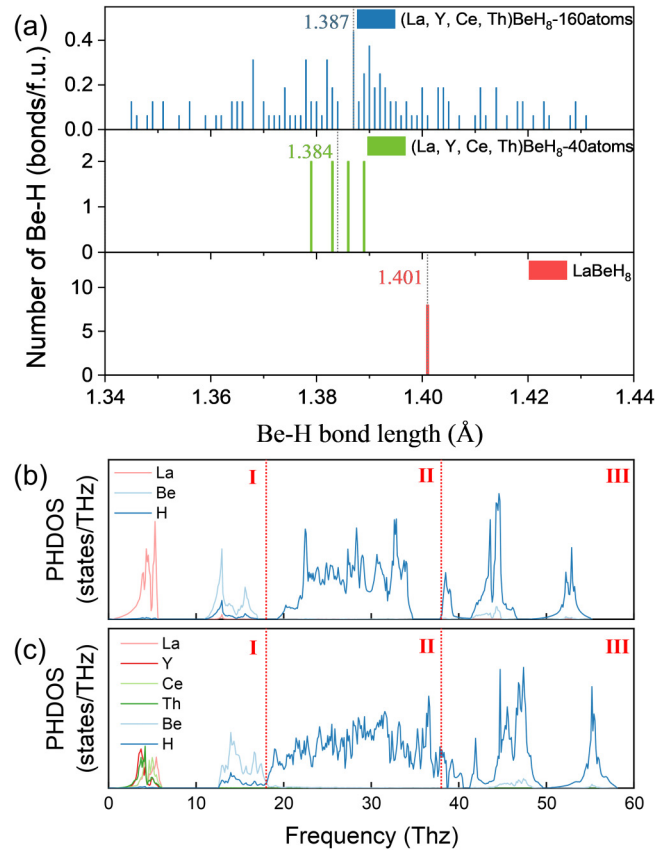

FIG. 6. (a) Histogram of Be–H bond length for (La, Y, Ce, Th)BeH_8 with 40 and 160 atoms, and $LaBeH_8$ at 100 GPa. The short dotted lines represent the average Be–H bond lengths in their respective structures. The comparison of projected phonon density of states (PHDOS) for (b) $LaBeH_8$ and (c) (La, Y, Ce, Th)BeH_8 at 100 GPa.

pressures of (La, Y, Ce, Th)BeH_8, we found phonon softening at *S*, *U*, and *T* points that induced the appearance of imaginary frequencies with decreasing pressure, as shown in Fig. 8, which are the origin of the instability at lower pressures. These results indicate that the stability of these alloy hydrides could be suppressed at low pressures.

C. Electronic properties

To investigate the chemical bonding characteristics of above-mentioned alloy hydrides and gain insight into their remarkable dynamic stability, we furthermore calculated the electron localization function (ELF) at 100 GPa. The absence of electron localization between distorted BeH_8 sublattice and randomly substituted metal sublattice suggests a clear ionic nature, plotted and shown in Fig. 9. Moreover, the Bader charge analysis (Table I) indicates that each H atom adopts approximately 0.40|e|, while each Be atom loses around 1.53|e|, resulting in a total charge of approximately 1.67|e| for each BeH_8 unit, which is close agreement with the charge transfer of BeH_8 in previous calculations for $XBeH_8$ (X = La, Y, Ce, and Th) [22,38]. The above analysis suggests that multielemental mixture does not alter the ionic bonding nature between the heavy metal and the BeH_8 units. In addition, the

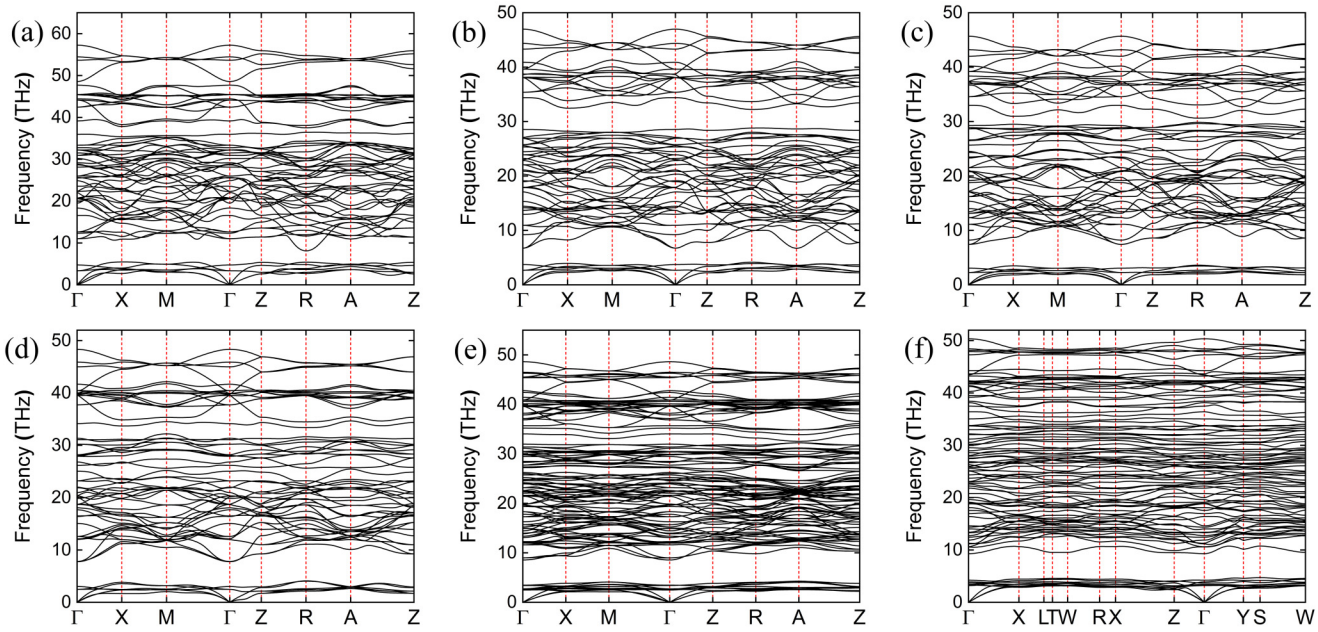

FIG. 7. Phonon-dispersion curves of alloy hydrides at their lowest dynamical pressures. (a) (La, Y)BeH_8 at 67 GPa, (b) (La, Ce)BeH_8 at 17 GPa, (c) (La, Th)BeH_8 at 10 GPa, (d) (Ce, Th)BeH_8 at 17 GPa, (e) (La, Ce, Th_2)BeH_8 at 20 GPa, and (f) (La, Ce, Th)BeH_8 at 30 GPa.

ELF with an isosurface value of 0.6 indicates a strong Be-H interaction, with Be–H bond lengths ranging from 1.379 to 1.422 Å at 100 GPa, fluctuating around the value of 1.401 Å (100 GPa) observed in $LaBeH_8$. The calculation of the negative ICOHP values for Be-H (approximately from −3.62 to −3.52 eV) reveals that the Be–H bonds in the BeH_8 units exhibit a significant covalent feature (Table II). In contrast, the H-H interactions are significantly weaker, as evidenced by their negative ICOHP values (−0.13 to −0.17 eV). The results show ionic bonding between distorted BeH_8 and the heavy-metal atoms, as well as the covalent bonding nature between Be and H within the BeH_8 unit in the multielement alloy system.

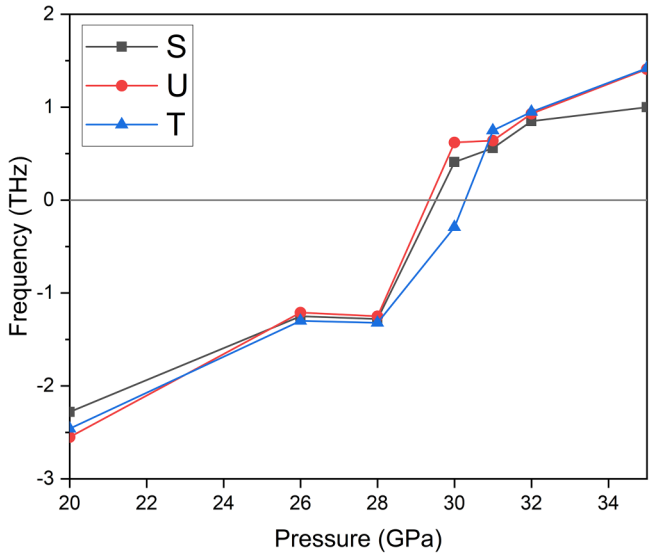

FIG. 8. Phonon frequencies for (La, Y, Ce, Th)BeH_8 as a function of pressure at highly symmetrical points, namely, $S = (0.5, 0.5, 0)$, $U = (0.5, 0, 0.5)$, and $T = (0, 0.5, 0.5)$.

D. Electron-phonon coupling and superconducting properties

The hydrides might possess high-T_c values because of the large H-dominated electronic density of states (DOS) at the Fermi level (E_F) and high-frequency H-derived vibrations. Our electronic calculations reveal that all predicted structures are metallic with significant electronic DOS at E_F [$N(E_F)$] for

TABLE I. Bader charge analysis for our predicted alloy hydrides at 100 GPa.

Formulas	H obtains charge	Be lost charge	Metal lost charge	
(La, Y)BeH_8	0.38	−1.53	La	−1.35
			Y	−1.70
(La, Ce)BeH_8	0.37	−1.53	La	−1.38
			Ce	−1.45
(La, Th)BeH_8	0.40	−1.55	La	−1.42
			Th	−1.82
(Ce, Th)BeH_8	0.40	−1.55	Ce	−1.47
			Th	−1.81
(La, Ce, Th)BeH_8	0.38	−1.53	La	−1.40
			Ce	−1.44
			Th	−1.76
(La, Ce, Th_2)BeH_8	0.39	−1.54	La	−1.39
			Ce	−1.46
			Th	−1.79
(La, Y, Ce, Th)BeH_8	0.39	−1.55	La	−1.33
			Y	−1.72
			Ce	−1.38
			Th	−1.73

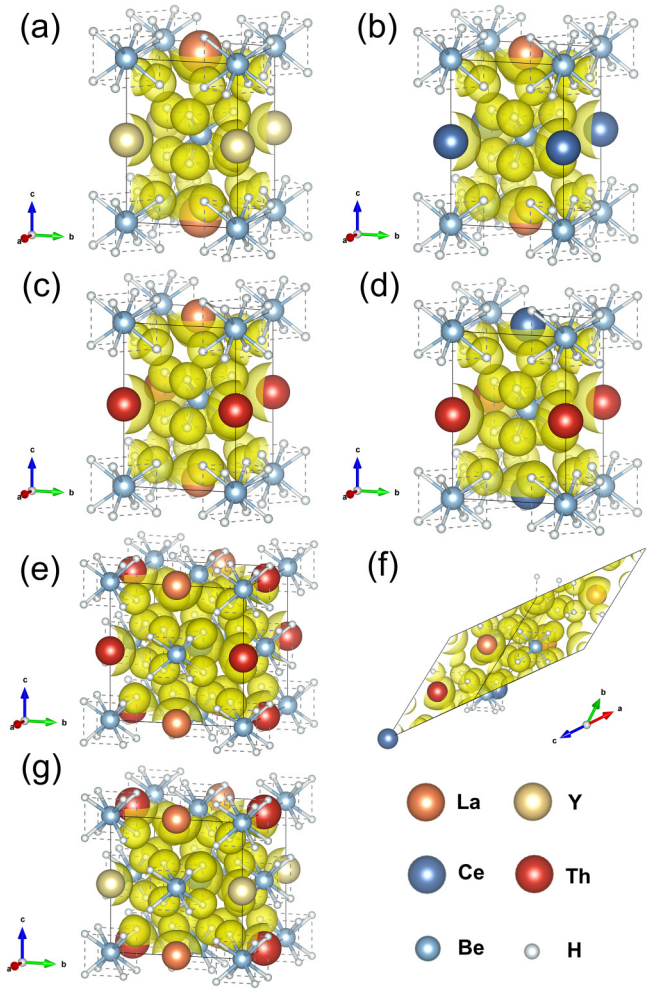

FIG. 9. Electron localization functions (ELFs) for (a) (La, Y)BeH_8, (b) (La, Ce)BeH_8, (c) (La, Th)BeH_8, (d) (Ce, Th)BeH_8, (e) (La, Ce, Th_2)BeH_8, (f) (La, Ce, Th)BeH_8, and (f) (La, Y, Ce, Th)BeH_8 at 100 GPa. The isosurface value is set to 0.6. Dashed lines are used to delineate BeH_8 units in alloy hydrides and do not represent actual chemical bonds.

hydrogen [see Fig. 12(b)] at 30 and 100 GPa, respectively. Hence, we performed electron-phonon coupling (EPC) simulations to investigate their superconductivity. As shown in the middle panels of Figs. 10 and 11(b), the projected phonon density of states (PHDOS) can be separated into three regions. The low-frequency region is dominated by contributions from heavy-metal atoms, while the mid- and high-frequency zones are associated with phonon modes of Be and H atoms, respectively. Simultaneously, large peaks in the $\alpha^2F(\omega)$ are distributed in the mid- and high-frequency regions, responsible for a rapid increase of high EPC strength, especially between 10–35 THz [Fig. 10 and Fig. 11(b)]. Consequently, the high EPC strength predominantly originates from the vibrations of hydrogen and Be atoms, and results in a total EPC parameter λ of 0.81, 0.94, 0.77, and 1.04 for (La, Ce)BeH_8 (77 GPa), (La, Th)BeH_8 (66 GPa), (La, Ce, Th)BeH_8 (60 GPa), and (La, Y, Ce, Th)BeH_8 (70 GPa), respectively.

Finally, we evaluate the T_c's by numerically solving the Migdal-Eliashberg equations directly; the obtained T_c values, along with the EPC parameter λ and the phonon frequency logarithmic average ω_{log} for these alloy hydrides, are shown in Table III. (La, Ce)BeH_8, (La, Th)BeH_8, and (La, Ce, Th)BeH_8 exhibit T_c values of 58–66 at 77 GPa, 83–92 K at 66 GPa, and 49–57 K at 60 GPa by using typical

TABLE II. The calculated ICOHP of H–H and Be–H bonds for our predicted alloy hydrides at 100 GPa. The negative ICOHP values represent the bonding interactions and positive ICOHP values represent the antibonding interactions.

Formulas	Distance of H–H and Be–H		ICOHP (eV)
(La, Y)BeH_8	H–H	1.451–1.654	−0.16
	Be–H	1.390–1.395	−3.62
(La, Ce)BeH_8	H–H	1.434–1.644	−0.14
	Be–H	1.390–1.401	−3.60
(La, Th)BeH_8	H–H	1.499–1.633	−0.13
	Be–H	1.398–1.411	−3.52
(Ce, Th)BeH_8	H–H	1.45–1.662	−0.13
	Be–H	1.401–1.403	−3.52
(La, Ce, Th)BeH_8	H–H	1.432–1.656	−0.17
	Be–H	1.384–1.422	−3.58
(La, Ce, Th_2)BeH_8	H–H	1.431–1.672	−0.14
	Be–H	1.379–1.389	−3.55
(La, Y, Ce, Th)BeH_8	H–H	1.446–1.656	−0.15
	Be–H	1.388–1.406	−3.58

TABLE III. The calculated EPC constant (λ), phonon frequency logarithmic average (ω_{log}), and superconducting critical temperature T_c ($\mu^* = 0.13$ and 0.1) by numerically solving the Eliashberg equations for various alloy structures under given pressures. For each alloy structure, the second pressure point is the lowest thermodynamic stability pressure, and the third pressure point is the lowest kinetic stability pressure.

Formulas	P (GPa)	λ	ω_{log} (K)	T_c (EA) (K)
(La, Y)BeH_8	100	1.88	986	188–195
	73	2.20	847	192–201
	50	3.18	621	204–213
(La, Ce)BeH_8	100	0.74	1226	53–65
	77	0.81	1136	58–66
	17	1.58	620	96–104
(La, Th)BeH_8	100	0.83	1277	66–81
	66	0.94	1148	83–92
	10	1.89	654	121–127
(Ce, Th)BeH_8	100	0.50	1242	14–22
	67	0.55	1086	13–19
	17	1.04	519	44–50
(La, Ce, Th)BeH_8	100	0.61	1281	23–32
	60	0.77	1061	49–57
	30	1.12	759	66–76
(La, Ce, Th_2)BeH_8	100	0.56	1259	20–28
	55	0.75	1057	48–55
	20	1.06	730	63–73
(La, Y, Ce, Th)BeH_8	100	0.89	1173	73–84
	70	1.04	1027	87–98
	32	1.68	635	104–112

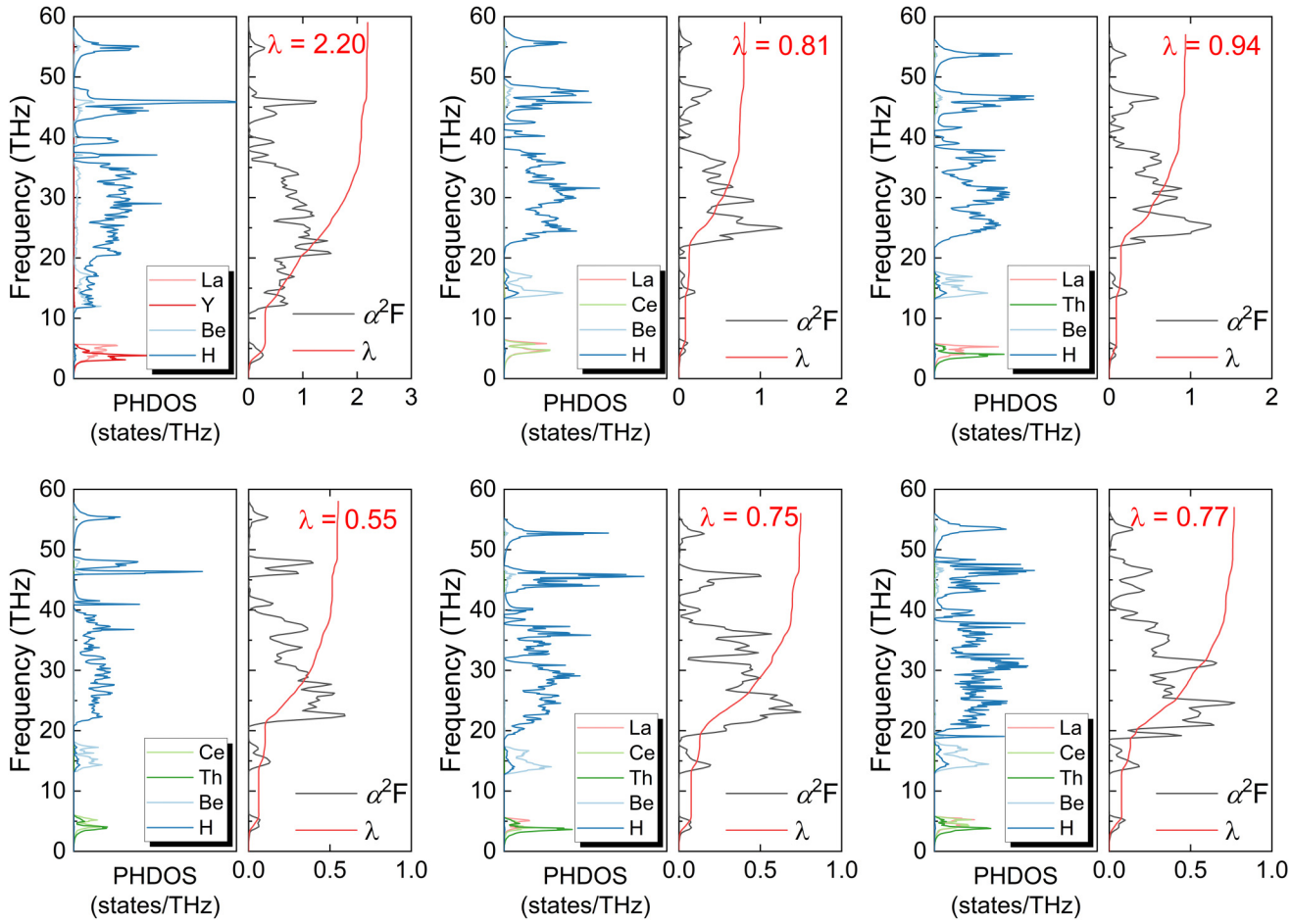

FIG. 10. PHDOS, Eliashberg spectral function $\alpha^2F(\omega)$, and the electron phonon integral $\lambda(\omega)$ for the alloy hydrides. (a) (La, Y)BeH_8 at 73 GPa, (b) (La, Ce)BeH_8 at 77 GPa, (c) (La, Th)BeH_8 at 66 GPa, (d) (Ce, Th)BeH_8 at 67 GPa, (e) (La, Ce, Th_2)BeH_8 at 55 GPa, and (f) (La, Ce, Th)BeH_8 at 60 GPa.

Coulomb pseudopotential parameters μ^* of 0.13–0.10. Notably, the T_c of (La, Y, Ce, Th)BeH_8 is estimated to range from 87 to 98 K ($\mu^* = 0.13 - 0.10$) at 70 GPa, exceeding the liquid nitrogen temperature of 77 K. The results further revealed that T_c and EPC parameter λ increase with decreasing pressure, while ω_{log} values show the opposite trend.

To investigate the origin of pressure dependence of superconductivity, we focus on establishing the correlation between superconductivity and electronic and phononic properties. As shown in the top panel of Fig. 12, the projected density of states (PDOS) calculations indicate that the $N(E_F)$ are primarily from the f- and d electrons of the heavy metals, as well as the dominant s electrons of hydrogen [Fig. 12(b)]. Among these, the contribution from the d electrons at the Fermi level is negligible, never exceeding 6% [Fig. 12(c)]. The variation of $N(E_F)$ in most alloy hydrides with respect to the pressure exhibits a positive pressure dependence, except for (La, Ce)BeH_8 and (Ce, Th)BeH_8 in Fig. 12(a). This behavior in (La, Ce)BeH_8 and (Ce, Th)BeH_8 arising from the significant contribution of Ce-4f electrons to $N(E_F)$ results in a negative pressure dependence of $N(E_F)$, as seen in Fig. 12(f), and a similar trend of $N(E_F)$ also observed in $CeBeH_8$ (see Ref. [37]). Neither La-4f nor Th-5f electrons exhibit a negative dependence on pressure [Figs. 12(e) and 12(g)]. As the proportion of Ce in the alloy decreases, its influence on $N(E_F)$ diminishes, and the $N(E_F)$ resumes the trend of decreasing with pressure decreasing, as seen in (La, Ce, Th_2)BeH_8 and (La, Y, Ce, Th)BeH_8 of Fig. 12(a). Crucially, however, the magnitude of $N(E_F)$ variation (whether positive or negative) remains minimal (e.g., <16% over 30–100 GPa) and cannot account for the dramatic pressure-induced changes of T_c. Another interesting observation is that the strong localization effect of Ce-4f electrons significantly suppresses superconductivity. Alloy systems with higher Ce-4f occupancy (e.g., (Ce, Th)BeH_8: 35% Ce-4f contribution at 100 GPa) exhibit anomalously low T_c (14–22 K), whereas Ce-free alloys like (La, Y)BeH_8 achieve T_c values up to 185–195 K under identical conditions.

The EPC calculations revealed that T_c and EPC parameter λ increase with decreasing pressure, while ω_{log} values show the opposite trend, which is attributed to the phonon softening arising from sizable distortion of the ideal cubic structure. For instance, in (La, Y, Ce, Th)BeH_8, we observe that with decreasing pressure, the phonon frequencies, especially for optical phonon modes, soften significantly across the entire Brillouin zone [Fig. 11(a)]; the corresponding Eliashberg spectral function $\alpha^2F(\omega)$ shifts from a 0–60-THz frequency range to 0–52 THz as pressure decreases in [Figs. 11(a)

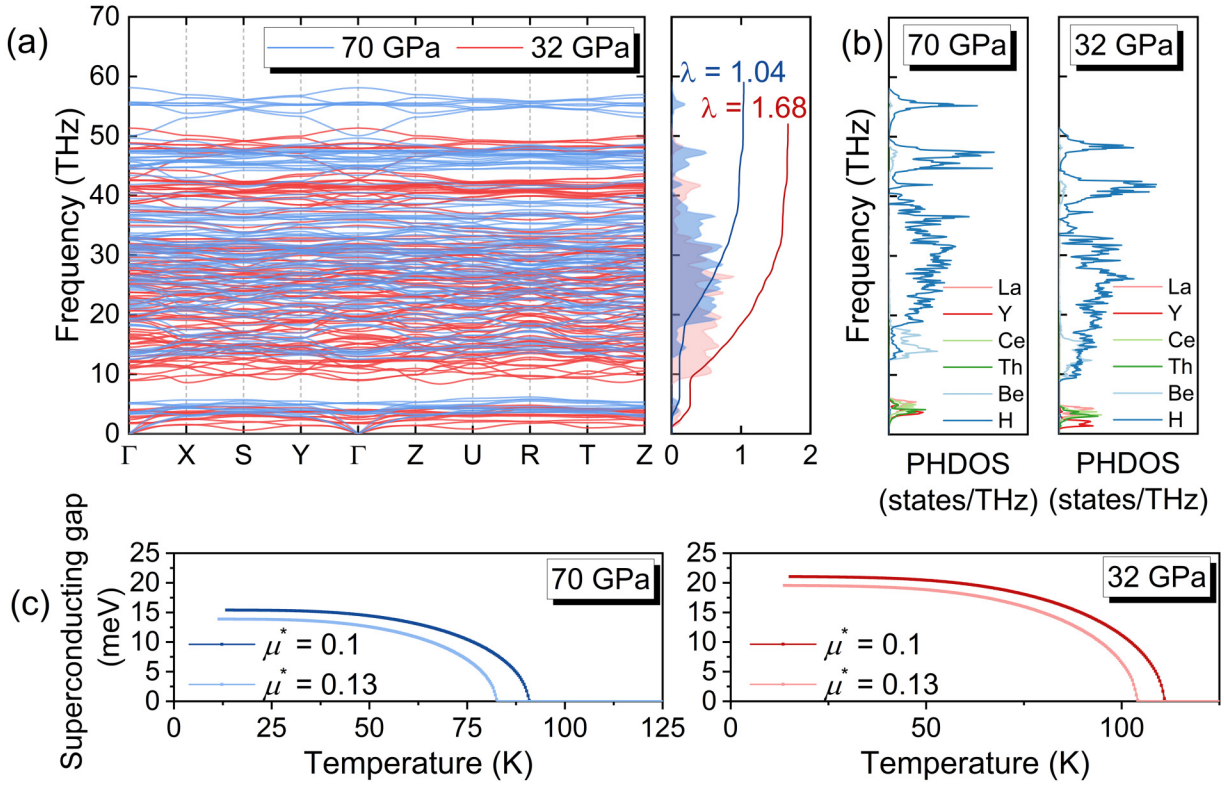

FIG. 11. (a) Phonon-dispersion curves, Eliashberg spectral function $\alpha^2F(\omega)$, and the electron-phonon integral $\lambda(\omega)$ for (La, Y, Ce, Th)BeH_8 at 70 (blue) and 32 GPa (red), respectively. (b) PHDOS and (c) calculated isotropic superconducting gap of (La, Y, Ce, Th)BeH_8 at 70 and 32 GPa, respectively.

and 11(b)]. This phonon softening significantly enhances λ from 1.04 to 1.68, driving a substantial 20% enhancement in T_c by solving isotropy Migdal-Eliashberg equations, highlighting the pivotal role of phonon behavior in modulating superconductivity under pressure. In addition, theoretical studies have indicated that the ultralight atomic mass of hydrogen in hydrides results in zero-point energy (ZPE)-driven lattice expansion, thereby affecting superconducting proper-

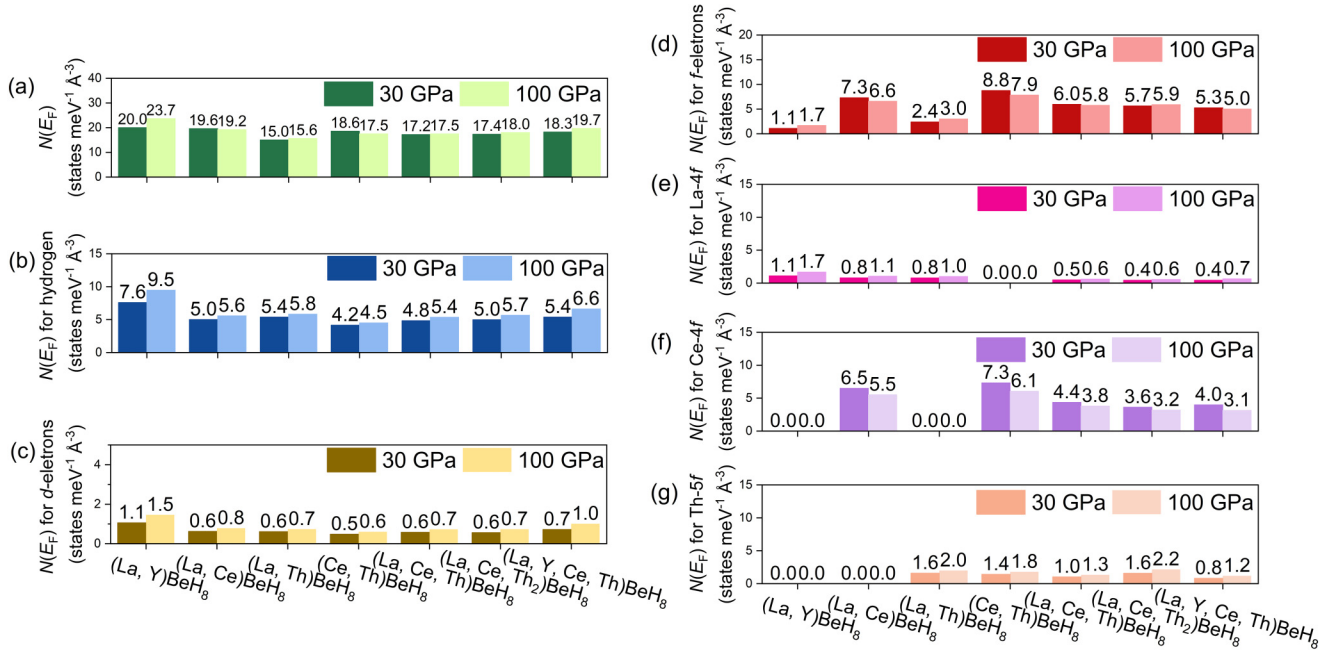

FIG. 12. The comparison of (a) the total $N(E_F)$, (b) $N(E_F)$ for hydrogen, (c) $N(E_F)$ for d electrons, (d) total f electrons, (e) $N(E_F)$ for La-4f electrons, (f) Ce-4f electrons, and (g) Th-5f electrons at 30 and 100 GPa.

ties. We have included the relevant discussion on this issue in Appendix D (including Refs. [76–80]).

IV. CONCLUSION

In summary, we combine La, Y, Ce, and Th elements in various ratios at the La sites within the parent structure $LaBeH_8$ to form alloy structures. To assess the realistic conditions of experimental synthesis, we estimate the stability of these predicted alloy hydrides by taking into account the important contribution of configurational and vibrational entropy to Gibbs free energy at high temperatures. (La, Ce)BeH_8, (La, Th)BeH_8, (La, Ce, Th)BeH_8, and (La, Y, Ce, Th)BeH_8 can maintain thermodynamic stability above 77, 66, 60, and 70 GPa at 2000 K, respectively. Our in-depth analysis indicates that vibrational entropy plays a much more significant role than configurational entropy in stabilizing these alloy hydrides, where configurational entropy has been widely regarded as a pivotal factor in the stability of multielemental alloy. Furthermore, EPC calculations reveal that all alloy hydrides have the potential to become superconductors within pressures of tens of GPa, especially for (La, Y, Ce, Th)BeH_8 with T_c of 87–98 K at 70 GPa. The simulations also suggest several hydrogen-based alloys with high T_c's above the liquid nitrogen temperature of 77 K at moderate pressures. Our findings shed light on the design and discovery of high-temperature superconductivity via multielemental alloy hydrides at near-ambient pressure conditions.

ACKNOWLEDGMENTS

This work was supported by the National Key Research and Development Program of China (Grants No. 2021YFA1400200, No. 2023YFA1608901, and No. 2023YFA1406002), National Natural Science Foundation of China (Grants No. 52288102, No. 52090024, No. 12474010, No. 12074139, No. 12374009, and No. T2494523011), the Program for Jilin University Computational Interdisciplinary Innovative Platform, Program for Jilin University Science and Technology Innovative Research Team (Grant No. 2021TD-05), the Fundamental Research Funds for the Central Universities, and computing facilities at the High-Performance Computing Centre of Jilin University.

APPENDIX A: CRYSTAL LATTICE PARAMETERS AND COORDINATES

In the pseudoquaternary system (La, Y, Ce, Th)BeH_8, the supercells generated by using the SQS method reveal the stability of the energy for alloy structures. This finding leads us to conclude that the short-range order of metal atoms does not significantly alter the description of disordered alloy hydrides. It further provides a rationale for employing small-sized unit cells to approximately evaluate the alloy properties, such as electronic properties and superconductivity.

The modeling of alloys with ratios of 1:1, 1:3, 1:1:2, and 1:1:1:1 is based on the $LaBeH_8$ unit cell, where La atoms are partially or totally substituted. Symmetry operations are applied to the substituted structures to obtain the minimal periodic units. In Table IV, (La, Th)BeH_8 and (La, Y, Ce, Th)BeH_8 are provided as examples. However, the quasiternary alloys with the ratio of 1:1:1 cannot be directly obtained through elemental substitution. To circumvent this limitation, we constructed a 30-atom SQS supercell based on the primitive cell of $LaBeH_8$. The disordered occupancy

TABLE IV. Crystal lattice parameters and coordinates of alloy hydrides at 100 GPa.

Phase	Lattice parameters		Coordinates		
*P*4/*mmm*-(La, Th)BeH_8	$a = 3.801$ $b = 3.801$ $c = 5.373$	La	0.500	0.500	0.000
		Th	0.000	0.000	0.500
		Be	0.000	0.000	0.000
		Be	0.500	0.500	0.500
		H	−0.301	0.000	0.150
		H	0.197	0.500	−0.348
*P*1-(La, Ce, Th)BeH_8	$a = 3.904$ $b = 5.540$ $c = 6.788$ $\alpha = 114.08°$ $\beta = 73.29°$ $\gamma = 89.90°$	La	−0.334	0.334	−0.333
		Th	0.333	−0.333	0.334
		Ce	0.000	−0.000	−0.001
		Be	0.333	0.167	0.333
		Be	0.001	0.499	−0.001
		Be	−0.334	−0.166	−0.331
		H	0.438	−0.081	0.124
		H	0.098	0.248	−0.195
		H	−0.236	−0.418	0.471
		H	−0.357	0.307	0.317
		H	0.293	−0.343	0.008
		H	−0.031	−0.014	−0.325
		H	0.237	0.109	−0.473
		H	−0.103	0.455	0.206
		H	−0.434	−0.214	−0.132
		H	0.041	0.307	0.317
		H	−0.301	−0.343	0.008
		H	0.356	−0.0142	−0.325
		H	0.0407	0.009	0.317
		H	−0.301	0.350	0.008
		H	0.356	−0.311	−0.325
		H	0.237	0.418	−0.473
		H	−0.103	−0.249	0.206
		H	−0.434	0.082	−0.132
		H	0.438	0.204	0.124
		H	0.098	−0.444	−0.195
		H	−0.236	−0.111	0.471
		H	−0.357	0.009	0.317
		H	0.293	0.350	0.008
		H	−0.031	−0.311	−0.325
Pmmm-(La, Y, Ce, Th)BeH_8	$a = 5.300$ $b = 5.298$ $c = 5.299$	La	0.500	0.000	0.000
		Y	0.000	0.500	0.000
		Ce	0.500	0.500	0.500
		Th	0.000	0.000	0.500
		Be	0.000	0.000	0.000
		Be	0.500	0.500	0.000
		Be	0.000	0.500	0.500
		Be	0.500	0.000	0.500
		H	−0.150	−0.155	−0.150
		H	0.348	0.352	−0.154
		H	−0.154	0.351	0.346
		H	0.348	−0.156	0.348

TABLE V. The symmetry assignment of the vibration modes at the Γ point in $LaBeH_8$ and (La, Y, Ce, Th)BeH_8.

	$LaBeH_8$		(La, Y, Ce, Th)BeH_8	
Area	Frequency (THz)	Symmetry	Frequency (THz)	Symmetry
I	1.31	T_{1u}	0.91, 1.01, 1.05	B_{2u}, B_{1u}, B_{3u}
	3.75	T_{1u}	3.35, 3.40, 3.41	B_{2u}, B_{3u}, B_{1u}
	3.82	T_{2u}	3.66, 3.66, 3.73	B_{1u}, B_{2u}, B_{3u}
	5.53	T_{1u}	5.00, 5.20, 5.21	B_{3u}, B_{1u}, B_{2u}
	11.62	T_{2u}	12.74, 12.87, 13.38	B_{3u}, B_{2u}, B_{1u}
	12.07	T_{1u}	13.56, 13.60, 13.94	B_{3u}, B_{2u}, B_{1u}
	13.62	T_{1u}	14.15, 14.23, 14.37	B_{2u}, B_{1u}, B_{3u}
	17.78	T_{1u}	18.28, 18.47, 18.52	B_{2u}, B_{3u}, B_{1u}
II	23.02–35.16	$4T_{1u}$, $3E_g$, $4T_{2g}$, $4T_{1g}$, $3E_u$, $4T_{2u}$, A_{2g}, A_{2u}, A_{1g}, A_{1u}	18.58–38.09	$8B_{1u}$, $8B_{2u}$, $8B_{3u}$, $8B_{1g}$, $8B_{2g}$, $8B_{3g}$, $8A_g$, $8A_u$
	38.72	A_{2u}	39.35	A_u
	38.76	E_u	40.31, 41.54	A_u, A_u
	41.83	T_{1u}	43.22, 44.25, 44.33	B_{2u}, B_{1u}, B_{3u}
	42.05	T_{2u}	44.59, 44.75, 45.49	B_{3u}, B_{1u}, B_{2u}
	43.93	T_{2g}	45.02, 45.06, 45.49	B_{1g}, B_{3g}, B_{2g}
	44.23	T_{1u}	46.60, 46.87, 46.96	B_{2u}, B_{3u}, B_{1u}
III	44.43	T_{1g}	46.01, 46.08, 46.20	B_{2g}, B_{3g}, B_{1g}
	44.52	T_{2g}	47.09, 47.19, 47.22	B_{1g}, B_{3g}, B_{2g}
	46.30	A_{1g}	47.23	A_g
	46.50	E_g	48.41, 49.33	A_g, A_g
	47.50	A_{2u}	49.87	A_u
	52.55	T_{1u}	55.00, 55.01, 55.05	B_{3u}, B_{1u}, B_{2u}
	53.18	T_{2g}	55.59, 55.66, 55.69	B_{2g}, B_{3g}, B_{1g}
	55.03	A_{1g}	57.98	A_{1g}

of heavy-metal atoms reduces the structure symmetry to $P1$ space group.

APPENDIX B: THERMODYNAMICS STABILITY ONLY WITH CONSIDERING CONFIGURATIONAL ENTROPY

In this Appendix, we systematically analyze the thermodynamic stability of $LaBeH_8$-type alloy hydrides by mixing multiple elements such as La, Y, Ce, and Th in different combinations and ratios (1:1, 1:3, 1:1:1, 2:1:1, and 1:1:1:1) in the pressure range of 50–300 GPa at 2000 K by PYMATGEN.

Our calculations reveal that in the absence of yttrium, the critical thermodynamic stability pressures of the alloy systems remain consistently below 100 GPa, regardless of the mixing combinations and ratios, as observed in La/Ce, La/Th, Ce/Th, and La/Ce/Th combinations, respectively [Figs. 13(b), 13(c), and 13(f)]. This finding aligns well with previous computational results. For instance, the thermodynamic stable pressures of superhydrides observed in the Y-H system are significantly higher than those in the La-H, Ce-H, and Th-H systems [70,72].

Below ∼100 GPa, we observe a sharp increase of the Gibbs free energy only considering configurational entropy, which is primarily driven by the interplay between configurational entropy and mixing formation enthalpy. For example, at a specified temperature (2000 K), the contribution of configurational entropy for 1:3 and 1:1 ratios remains constant of 9.7 and 11.9 meV per atom, respectively. In contrast, the mixing formation enthalpy is governed by the enthalpy difference between the alloy hydrides and other decomposed products. As the pressure decreases, the emergence of decomposed products with lower enthalpy leads to a mixing formation enthalpy curve of alloys characterized by a steep increase at low pressures and a gentler variation at high pressures. Consequently, the limited contribution of configurational entropy restricts the reduction of the thermodynamic stabilization pressure to ∼100 GPa.

APPENDIX C: THE SYMMETRY ANALYSIS OF THE VIBRATION MODES AT THE Γ POINT IN $LaBeH_8$ AND (La, Y, Ce, Th)BeH_8

In comparison, the phonon vibrational frequencies of the alloy (La, Y, Ce, Th)BeH_8 in region I and region III are close to the frequencies of $LaBeH_8$ due to lattice distortion, and there is a clear correspondence in the splitting of the vibrational modes. The split vibrational modes in (La, Y, Ce, Th)BeH_8 do not exhibit significant energy-level crossing. However, in region II, the energy levels of the split vibrational modes in (La, Y, Ce, Th)BeH_8 have a complex interleaving relationship compared with those in $LaBeH_8$ (Table V).

APPENDIX D: THE EQUATION OF STATE OF (La, Y, Ce, Th)BeH_8 WITH OR WITHOUT ZPE

In our studied alloy hydrides, the superconducting properties are influenced not only by the $N(E_F)$ and phonon soft modes, but also significantly by ZPE-induced lattice expansion. The extremely small atomic mass of hydrogen leads to high-frequency vibrations with high phonon energies, such as ∼250 meV (∼60 THz) in (La, Y, Ce, Th)BeH_8 at 70 GPa, making the ZPE contribution to the total energy non-negligible.

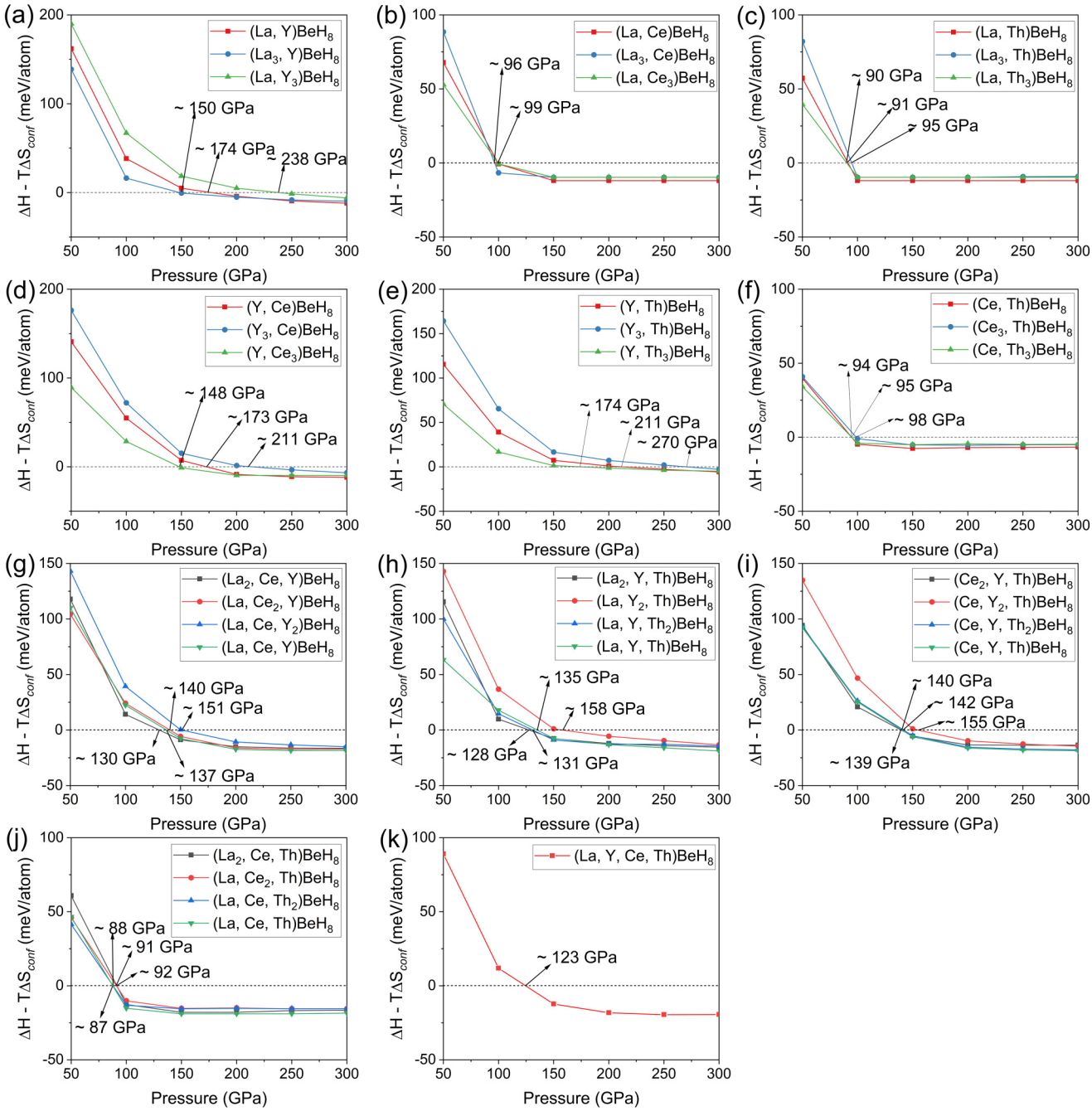

FIG. 13. Calculated Gibbs free energy as a function of pressure considering the contribution of ΔS_{conf} at 2000 K for quasibinary, quasiternary, and quasiquaternary alloy hydrides.

Calculated phonon density of states (PHDOS) are used to evaluate the zero-point energy (ZPE) correction within the quasiharmonic approximation, and the calculated static energies with or without ZPE by first-principles with respect to the volume are fitted to the third-order Birch-Murnaghan equation of state [76] by formulas (D1) and (D2):

$$P(V) = \frac{3B_0}{2}[(V_0/V)^{7/3} - (V_0/V)^{5/3}]^3 \times \left\{1 + \frac{3}{4}(B_0' - 4)[(V_0/V)^{2/3} - 1]\right\}, \quad \text{(D1)}$$

$$E(V) = E_0 + \frac{9V_0B_0}{16}\{[(V_0/V)^{2/3} - 1]^3 B_0' + [(V_0/V)^{2/3} - 1]^2[6 - 4(V_0/V)^{2/3}]\}. \quad \text{(D2)}$$

For instance, in our calculations of (La, Y, Ce, Th)BeH_8 systems, equation of state (EOS) comparisons reveal that inclusion of ZPE leads to lattice expansion. Within the pressure range from 60 to 100 GPa, we observe an average volume expansion of ~3.3%, and the expansion rate increases as pressure lowers (Fig. 14). Indeed, some theoretical

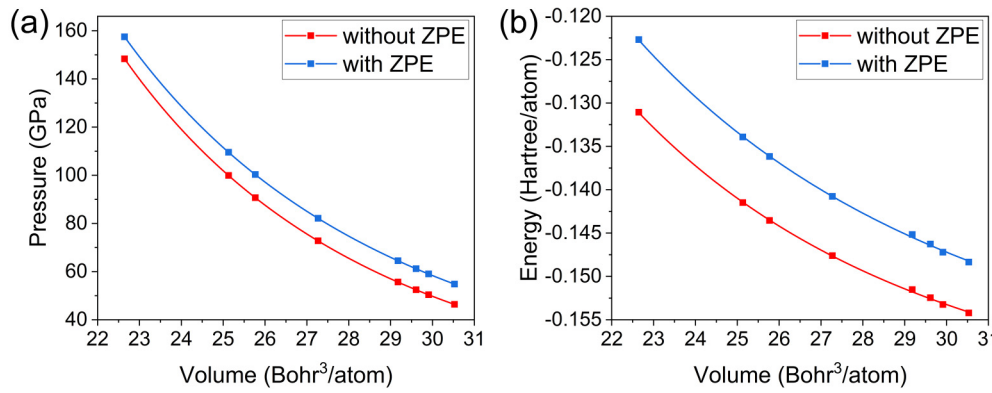

FIG. 14. The comparison of the (a) pressure-volume curves and (b) energy-volume curves with (blue) and without (red) considering the ZPE (zero-point energy).

simulations reveal that the impact of ionic vibration-induced lattice expansion on superconductivity can be considered within the quasiharmonic approximation [77], but a potentially sizable frequency renormalization caused by anharmonic and phonon-phonon effects of ionic vibration is neglected, which might significantly influence superconductivity [78,80]. Therefore, our work does not include the discussion of quantum ionic effect on superconductivity, and we expect further experimental developments to justify corresponding simulations.

[1] H. Wang, X. Li, G. Gao, Y. Li, and Y. Ma, Hydrogen-rich superconductors at high pressures, WIREs Comput. Mol. Sci. **8**, e1330 (2018).

[2] J. Lv, Y. Sun, H. Liu, and Y. Ma, Theory-orientated discovery of high-temperature superconductors in superhydrides stabilized under high pressure, Matter Radiat. Extremes **5**, 068101 (2020).

[3] J. A. Flores-Livas, L. Boeri, A. Sanna, G. Profeta, R. Arita, and M. Eremets, A perspective on conventional high-temperature superconductors at high pressure: Methods and materials, Phys. Rep. **856**, 1 (2020).

[4] X. Zhang, Y. Zhao, F. Li, and G. Yang, Pressure-induced hydride superconductors above 200 K, Matter Radiat. Extremes **6**, 068201 (2021).

[5] Y. Sun, X. Zhong, H. Liu, and Y. Ma, Clathrate metal superhydrides at high-pressure conditions: Enroute to room-temperature superconductivity, Natl. Sci. Rev. **11**, nwad270 (2023).

[6] X. Zhong, J. S. Tse, R. J. Hemley, and H. Liu, Theory-directed discovery of high-temperature superconductivity in clathrate hydrides at high pressure, The Inovation **3**, 100226 (2022).

[7] A. P. Drozdov, M. I. Eremets, I. A. Troyan, V. Ksenofontov, and S. I. Shylin, Conventional superconductivity at 203 kelvin at high pressures in the sulfur hydride system, Nature (London) **525**, 73 (2015).

[8] M. Einaga, M. Sakata, T. Ishikawa, K. Shimizu, M. I. Eremets, A. P. Drozdov, I. A. Troyan, N. Hirao, and Y. Ohishi, Crystal structure of the superconducting phase of sulfur hydride, Nat. Phys. **12**, 835 (2016).

[9] L. Ma, K. Wang, Y. Xie, X. Yang, Y. Wang, M. Zhou, H. Liu, X. Yu, Y. Zhao, H. Wang, G. Liu, and Y. Ma, High-temperature superconducting phase in clathrate calcium hydride CaH_6 up to 215 K at a pressure of 172 GPa, Phys. Rev. Lett. **128**, 167001 (2022).

[10] Z. Li *et al.*, Superconductivity above 200 K discovered in superhydrides of calcium, Nat. Commun. **13**, 2863 (2022).

[11] P. Kong, V. S. Minkov, M. A. Kuzovnikov, A. P. Drozdov, S. P. Besedin, S. Mozaffari, L. Balicas, F. F. Balakirev, V. B. Prakapenka, S. Chariton, D. A. Knyazev, E. Greenberg, and M. I. Eremets, Superconductivity up to 243 K in the yttrium-hydrogen system under high pressure, Nat. Commun. **12**, 5075 (2021).

[12] I. A. Troyan, D. V. Semenok, A. G. Kvashnin, A. V. Sadakov, O. A. Sobolevskiy, V. M. Pudalov, A. G. Ivanova, V. B. Prakapenka, E. Greenberg, A. G. Gavriliuk, I. S. Lyubutin, V. V. Struzhkin, A. Bergara, I. Errea, R. Bianco, M. Calandra, F. Mauri, L. Monacelli, R. Akashi, and A. R. Oganov, Anomalous high-temperature superconductivity in YH_6, Adv. Mater. **33**, 2006832 (2021).

[13] M. Somayazulu, M. Ahart, A. K. Mishra, Z. M. Geballe, M. Baldini, Y. Meng, V. V. Struzhkin, and R. J. Hemley, Evidence for superconductivity above 260 K in lanthanum superhydride at megabar pressures, Phys. Rev. Lett. **122**, 027001 (2019).

[14] A. P. Drozdov, P. P. Kong, V. S. Minkov, S. P. Besedin, M. A. Kuzovnikov, S. Mozaffari, L. Balicas, F. F. Balakirev, D. E. Graf, V. B. Prakapenka, E. Greenberg, D. A. Knyazev, M. Tkacz, and M. I. Eremets, Superconductivity at 250 K in lanthanum hydride under high pressures, Nature (London) **569**, 528 (2019).

[15] I. A. Kruglov, A. G. Kvashnin, A. F. Goncharov, A. R. Oganov, S. S. Lobanov, N. Holtgrewe, S. Q. Jiang, V. B. Prakapenka, E. Greenberg, and A. V. Yanilkin, Uranium polyhydrides at moderate pressures: Prediction, synthesis, and expected superconductivity, Sci. Adv. **4**, eaat9776 (2018).

[16] D. Zhou, D. V. Semenok, D. Duan, H. Xie, W. Chen, X. Huang, X. Li, B. Liu, A. R. Oganov, and T. Cui, Superconducting praseodymium superhydrides, Sci. Adv. **6**, eaax6849 (2020).

[17] X. Li, X. Huang, D. Duan, C. J. Pickard, D. Zhou, H. Xie, Q. Zhuang, Y. Huang, Q. Zhou, B. Liu, and T. Cui, Polyhydride

CeH_9 with an atomic-like hydrogen clathrate structure, Nat. Commun. **10**, 3461 (2019).

[18] W. Chen, D. V. Semenok, X. Huang, H. Shu, X. Li, D. Duan, T. Cui, and A. R. Oganov, High-Temperature superconducting phases in cerium superhydride with a T_c up to 115 K below a pressure of 1 megabar, Phys. Rev. Lett. **127**, 117001 (2021).

[19] N. P. Salke, M. M. D. Esfahani, Y. Zhang, I. A. Kruglov, J. Zhou, Y. wang, E. Greenberg, V. B. Prakapenka, J. Liu, A. R. Oganov, and J. Lin, Synthesis of clathrate cerium superhydride CeH_9 at 80–100 GPa with atomic hydrogen sublattice, Nat. Commun. **10**, 4453 (2019).

[20] S. Di Cataldo, C. Heil, W. von der Linden, and L. Boeri, $LaBH_8$: Towards high-T_c low-pressure superconductivity in ternary superhydrides, Phys. Rev. B **104**, L020511 (2021).

[21] X. Liang, A. Bergara, X. Wei, X. Song, L. Wang, R. Sun, H. Liu, R. J. Hemley, L. Wang, G. Gao, and Y. Tian, Prediction of high-T_c superconductivity in ternary lanthanum borohydrides, Phys. Rev. B **104**, 134501 (2021).

[22] Z. Zhang, T. Cui, M. J. Hutcheon, A. M. Shipley, H. Song, M. Du, V. Z. Kresin, D. Duan, C. J. Pickard, and Y. Yao, Design principles for high-temperature superconductors with a hydrogen-based alloy backbone at moderate pressure, Phys. Rev. Lett. **128**, 047001 (2022).

[23] Y. Song, J. Bi, Y. Nakamoto, K. Shimizu, H. Liu, B. Zou, G. Liu, H. Wang, and Y. Ma, Stoichiometric ternary superhydride $LaBeH_8$ as a new template for high-temperature superconductivity at 110 K under 80 GPa, Phys. Rev. Lett. **130**, 266001 (2023).

[24] K. Dolui, L. J. Conway, C. Heil, T. A. Strobel, R. P. Prasankumar, and C. J. Pickard, Feasible route to high-temperature ambient-pressure hydride superconductivity, Phys. Rev. Lett. **132**, 166001 (2024).

[25] A. Sanna, T. F. T. Cerqueira, Y. Fang, I. Errea, A. Ludwig, and M. A. L. Marques, Prediction of ambient pressure conventional superconductivity above 80 K in hydride compounds, npj Comput. Mater. **10**, 44 (2024).

[26] E. P. George, D. Raabe, and R. O. Ritchie, High-entropy alloys, Nat. Rev. Mater. **4**, 515 (2019).

[27] B. Ouyang and Y. Zeng, The rise of high-entropy battery materials, Nat. Commun. **15**, 973 (2024).

[28] J. Bi, Y. Nakamoto, P. Zhang, Y. Wang, L. Ma, Y. Wang, B. Zou, K. Shimizu, H. Liu, M. Zhou, H. Wang, G. Liu, and Y. Ma, Stabilization of superconductive La-Y alloy superhydride with T_c above 90 K at megabar pressure, Mater. Today Phys. **28**, 100840 (2022).

[29] X. Liang, X. Wei, E. Zurek, A. Bergara, P. Li, G. Gao, and Y. Tian, Design of high-temperature superconductors at moderate pressures by alloying AlH_3 or GaH_3, Matter Radiat. Extremes **9**, 018401 (2024).

[30] D. V. Semenok, I. A. Troyan, A. G. Ivanova, A. G. Kvashnin, I. A. Kruglov, M. Hanfland, A. V. Sadakov, O. A. Sobolevskiy, K. S. Pervakov, I. S. Lyubutin, K. V. Glazyrin, N. Giordano, D. N. Karimov, A. L. Vasiliev, R. Akashi, V. M. Pudalov, and A. R. Oganov, Superconductivity at 253 K in lanthanum–yttrium ternary hydrides, Mater. Today **48**, 18 (2021).

[31] J. Bi, Y. Nakamoto, P. Zhang, K. Shimizu, B. Zou, H. Liu, M. Zhou, G. Liu, H. Wang, and Y. Ma, Giant enhancement of superconducting critical temperature in substitutional alloy (La, Ce)H_9, Nat. Commun. **13**, 5952 (2022).

[32] W. Chen, X. Huang, D. V. Semenok, S. Chen, D. Zhou, K. Zhang, A. R. Oganov, and T. Cui, Enhancement of superconducting properties in the La–Ce–H system at moderate pressures, Nat. Commun. **14**, 2660 (2023).

[33] S. Chen, Y. Qian, X. Huang, W. Chen, J. Guo, K. Zhang, J. Zhang, H. Yuan, and T. Cui, High-temperature superconductivity up to 223 K in the Al stabilized metastable hexagonal lanthanum superhydride, Natl. Sci. Rev. **11**, nwad107 (2024).

[34] D. V. Semenok, I. A. Troyan, A. V. Sadakov, D. Zhou, M. Galasso, A. G. Kvashnin, A. G. Ivanova, I. A. Kruglov, A. A. Bykov, K. Y. Terent'ev, A. V. Cherepakhin, O. A. Sobolevskiy, K. S. Pervakov, A. Yu. Seregin, T. Helm, T. Förster, A. D. Grockowiak, S. W. Tozer, Y. Nakamoto, K. Shimizu *et al.*, Effect of magnetic impurities on superconductivity in LaH_{10}, Adv. Mat. **34**, 2204038 (2022).

[35] G. Huang, D. Peng, T. Luo, L. Chen, P. D. Simpson, Z. Cao, F. A. Gorelli, G. Zhong, H. Lin, and X. Chen, Synthesis of superconducting phase of $La_{0.5}Ce_{0.5}H_{10}$ at high pressures, J. Phys.: Condens. Matter **36**, 075702 (2024).

[36] S. Chen, Y. Wang, F. Bai, X. Wu, X. Wu, A. Pakhomova, J. Guo, X. Huang, and T. Cui, Superior superconducting properties realized in quaternary La−Y−Ce hydrides at moderate pressures, J. Am. Chem. Soc. **146**, 14105 (2024).

[37] Y. Sun, S. Sun, X. Zhong, and H. Liu, Prediction for high superconducting ternary hydrides below megabar pressure, J. Phys.: Condens. Matter **34**, 505404 (2022).

[38] Q. Jiang, Z. Zhang, H. Song, Y. Ma, Y. Sun, M. Mao, T. Cui, and D. Duan, Ternary superconducting hydrides stabilized via Th and Ce elements at mild pressures, Fundam. Res. **4**, 550 (2022).

[39] K. Gao, W. Cui, J. Shi, A. P. Durajski, J. Hao, S. Botti, M. A. L. Marques, and Y. Li, Prediction of high-T_c superconductivity in ternary actinium beryllium hydrides at low pressure, Phys. Rev. B **109**, 014501 (2024).

[40] B. Li, Y. Yang, Y. Fan, C. Zhu, S. Liu, and Z. Shi, Theoretical predictions on superconducting phase above room Temperature in lutetium-beryllium hydrides at high pressures, Chin. Phys. Lett. **40**, 097402 (2023).

[41] J. Du, Q. Jiang, Z. Zhang, W. Zhao, L. Chen, Z. Huo, H. Song, F. Tian, D. Duan, and T. Cui, First-principles study of high-pressure structural phase transition and superconductivity of $YBeH_8$, J. Chem. Phys. **160**, 094116 (2024).

[42] W. Zhao, D. Duan, D. An, Q. Jiang, Z. Liu, T. Ma, Z. Huo, J. Du, and T. Cui, High temperature superconductivity of quaternary hydrides $XM_3Be_4H_{32}$ (X, M = Ca, Sr, Ba, Y, La, Ac, Th) under moderate pressure, Mater. Today Phys. **43**, 101387 (2024).

[43] G. Kresse and J. Furthmüller, Efficient iterative schemes for *ab initio* total-energy calculations using a plane-wave basis set, Phys. Rev. B **54**, 11169 (1996).

[44] W. Kohn and L. J. Sham, Self-Consistent equations including exchange and correlation effects, Phys. Rev. **140**, A1133 (1965).

[45] J. P. Perdew, K. Burke, and M. Ernzerhof, Generalized gradient approximation made simple, Phys. Rev. Lett. **77**, 3865 (1996).

[46] P. E. Blöchl, Projector augmented-wave method, Phys. Rev. B **50**, 17953 (1994).

[47] S. P. Ong, W. D. Richards, A. Jain, G. Hautier, M. Kocher, S. Cholia, D. Gunter, V. L. Chevrier, K. A. Persson, and G. Ceder, Python materials genomics (pymatgen): A robust, open-source python library for materials analysis, Comput. Mater. Sci. **68**, 314 (2013).

[48] R. Dronskowski and P. E. Bloechl, Crystal orbital Hamilton populations (COHP): Energy-resolved visualization of chemical bonding in solids based on density-functional calculations, J. Phys. Chem. **97**, 8617 (1993).

[49] V. L. Deringer, A. L. Tchougréeff, and R. Dronskowski, Crystal orbital Hamilton population (COHP) analysis as projected from planewave basis sets, J. Phys. Chem. A **115**, 5461 (2011).

[50] S. Maintz, V. L. Deringer, A. L. Tchougre, and R. Dronskowski, LOBSTER: A tool to extract chemical bonding from plane-wave based DFT, J. Comput. Chem. **37**, 1030 (2016).

[51] R. F. W. Bader, Atoms in molecules, Acc. Chem. Res. **18**, 9 (1985).

[52] A. D. Becke and K. E. Edgecombe, A simple measure of electron localization in atomic and molecular-systems, J. Chem. Phys. **92**, 5397 (1990).

[53] S. Baroni, S. De Gironcoli, A. Dal Corso, and P. Giannozzi, Phonons and related crystal properties from density-functional perturbation theory, Rev. Mod. Phys. **73**, 515 (2001).

[54] P. Giannozzi, S. Baroni, N. Bonini, M. Calandra, R. Car, C. Cavazzoni, D. Ceresoli, G. L. Chiarotti, M. Cococcioni, I. Dabo *et al.*, QUANTUM ESPRESSO: A modular and open-source software project for quantum simulations of materials, J. Phys.: Condens. Matter **21**, 395502 (2009).

[55] G. Eliashberg, Interactions between electrons and lattice vibrations in a superconductor, Sov. Phys. JETP **11**, 696 (1960).

[56] J. P. Carbotte, Properties of boson-exchange superconductors, Rev. Mod. Phys. **62**, 1027 (1990).

[57] A. Sanna, J. A. Flores-Livas, A. Davydov, G. Profeta, K. Dewhurst, S. Sharma, and E. Gross, *Ab initio* Eliashberg theory: Making genuine predictions of superconducting features, J. Phys. Soc. Jpn. **87**, 041012 (2018).

[58] The ELK code, http://elk.sourceforge.net.

[59] A. Zunger, S.-H. Wei, L. G. Ferreira, and J. E. Bernard, Special quasirandom structures, Phys. Rev. Lett. **65**, 353 (1990).

[60] A. van de Walle, M. Asta, and G. Ceder, The alloy theoretic automated toolkit: A user guide, Calphad **26**, 539 (2002).

[61] A. Togo and I. Tanaka, First principles phonon calculations in materials science, Scr. Mater. **108**, 1 (2015).

[62] B. Fultz, Vibrational thermodynamics of materials, Prog. Mater Sci. **55**, 247 (2010).

[63] S. Nosé, A unified formulation of the constant temperature molecular dynamics methods, J. Chem. Phys. **81**, 511 (1984).

[64] S. Nosé, Constant temperature molecular dynamics methods, Prog. Theor. Phys. Suppl. **103**, 1 (1991).

[65] W. G. Hoover, Canonical dynamics: Equilibrium phase-space distributions, Phys. Rev. A **31**, 1695 (1985).

[66] M. Widom, W. Huhn, S. Maiti, and W. Steurer, Hybrid Monte Carlo/molecular dynamics simulation of a refractory metal high entropy alloy, Metall. Mater. Trans. A **45**, 196 (2014).

[67] S. Plimpton, Fast parallel algorithms for short-range molecular dynamics, J. Comput. Phys. **117**, 1 (1995).

[68] A. P. Thompson, H. M. Aktulga, R. Berger, D. S. Bolintineanu, W. M. Brown, P. S. Crozier, P. J. in't Veld, A. Kohlmeyer, S. G. Moore, T. D. Nguyen *et al.*, LAMMPS - a flexible simulation tool for particle-based materials modeling at the atomic, meso, and continuum scales, Comput. Phys. Comm. **271**, 108171 (2022).

[69] T. Hanke, A. L. Upterworth, and D. Sebastiani, Explicit configurational entropy of mixing in molecular dynamics simulations, J. Phys. Chem. Lett. **15**, 11320 (2024).

[70] F. Peng, Y. Sun, C. J. Pickard, R. J. Needs, Q. Wu, and Y. Ma, Hydrogen clathrate structures in rare earth hydrides at high pressures: Possible route to room-temperature superconductivity, Phys. Rev. Lett. **119**, 107001 (2017).

[71] H. Liu, I. I. Naumova, R. Hoffmann, N. W. Ashcroft, and R. J. Hemley, Potential high-T_c superconducting lanthanum and yttrium hydrides at high pressure, Proc. Natl. Acad. Sci. USA **114**, 6990 (2017).

[72] A. G. Kvashnin, D. V. Semenok, I. A. Kruglov, I. A. Wrona, and A. R. Oganov, High-temperature superconductivity in a Th−H system under pressure conditions, ACS Appl. Mater. Interfaces **10**, 43809 (2018).

[73] X.-L. He, P. Zhang, Y. Ma, H. Li, X. Zhong, Y. Wang, H. Liu, and Y. Ma, Potential high-temperature superconductivity in the substitutional alloy of (Y, Sr)H_{11} under high pressure, Phys. Rev. B **107**, 134509 (2023).

[74] Z. Wang, H. Zhao, X. Zhong, H. Liu, and Y. Ma, Unlocking the origin of stability and superconductivity in $LaBeH_8$ at submegabar pressure, Phys. Rev. B **109**, 214506 (2024).

[75] Y. Wang, X. Li, J. Luo, B. F. Woodfield, X. Wang, T. Feng, N. Yin, Q. Shi, G. Li, and L. Li, An unexpected decrease in vibrational entropy of multicomponent rutile oxides, J. Am. Chem. Soc. **146**, 14493 (2024).

[76] F. Birch, Finite elastic strain of cubic crystals, Phys. Rev. **71**, 809 (1947).

[77] M. A. Olea-Amezcua, O. De la Peña-Seaman, and R. Heid, Superconductivity by doping in alkali-metal hydrides without applied pressure: An *ab initio* study, Phys. Rev. B **99**, 214504 (2019).

[78] F. Belli and I. Errea, Impact of ionic quantum fluctuations on the thermodynamic stability and superconductivity of $LaBH_8$, Phys. Rev. B **106**, 134509 (2022).

[79] P. Hou, F. Belli, R. Bianco, and I. Errea, Quantum anharmonic enhancement of superconductivity in $P6_3/mmc$ ScH_6 at high pressures: A first-principles study, J. Appl. Phys. **130**, 175902 (2021).

[80] I. Errea, F. Belli, L. Monacelli, A. Sanna, T. Koretsune, T. Tadano, R. Bianco, M. Calandra, R. Arita, F. Mauri, and J. A. Flores-Livas, Quantum crystal structure in the 250-kelvin superconducting lanthanum hydride, Nature (London) **578**, 66 (2020).